



Hysteresis quantified control for switched reaction–diffusion systems and its application

Zenglong Peng¹ · Xiaona Song¹ · Shuai Song¹ · Vladimir Stojanovic²

Received: 7 February 2023 / Accepted: 3 June 2023
© The Author(s) 2023

Abstract

This article addresses the exponential input-to-state stabilization problem for switched reaction–diffusion systems, in which the systems' mode jumping complies with the persistent dwell-time switching mechanism. On the basis of point measurement, a novel pointwise controller is designed to reduce the amount of sensors and actuators. Then, a hysteresis quantizer with an adjustable parameter is employed to balance the quantitative effect and system's performance, which can improve the bandwidth utilization of the network, simultaneously. Finally, the effectiveness of the proposed approach is demonstrated by an application of the temperature control of power semiconductor chips.

Keywords Exponential input-to-state stabilization · Hysteresis quantizer · Switched reaction–diffusion systems · Persistent dwell-time · Power semiconductor chips.

Introduction

In reality, one of the most significant tasks in the analysis and synthesis of control systems is the development of an accurate mathematical model, which can properly represent the dynamic behavior of systems. In this context, reaction–diffusion systems (RDSs), as an effective model for characterizing the performance of space-time related dynamic systems, appear in recent literature [1–6]. This trend is driven by RDSs' numerous practical applications, which include various fields such as chemical, nuclear, aerospace [7], etc. To date, fruitful research results have been achieved in the field of RDSs control, such as event-triggered con-

trol [1], saturated control [8], boundary control [9, 10], and output feedback control [11]. It is noteworthy that the above works predominantly focused on single-mode RDSs (RDSs with only one mode). Without a doubt there will be a non-negligible fact that some practical systems are frequently influenced by external uncertainties that lead such systems to exhibit multiple modes [12–14], which makes single-mode RDSs challenging in describing more general physical processes. In this regard, how to establish accurate mathematical models for some more complicated and realistic multi-mode systems by reaction-diffusion models is a topic worth exploring.

As reported in the existing works [12, 15], switched RDSs with certain switching mechanisms play an important role in describing systems that exhibit multi-mode characteristics and spatial features. Consequently, on the basis of switched RDSs, it is particularly important to explore the switching mechanisms contained in the subsystems. In accordance with this research direction, Refs. [16, 17] made the first attempts to propose dwell-time (DT) and average dwell-time (ADT) switching mechanisms to describe the switching laws obeyed by the subsystems. Subsequently, due to the limitations of DT's dwell time and ADT's switching frequency, they are unable to describe the fast switching phenomenon, which is common in some practical systems, such as complex dynamic networks [18] and mass-spring systems [19]. Based on this fact, an extended persistent dwell-time (PDT)

✉ Vladimir Stojanovic
vladostojanovic@mts.rs

Zenglong Peng
zlpeng2022@163.com

Xiaona Song
xiaona_97@163.com

Shuai Song
songshuai_1010@163.com

¹ School of Information Engineering, Henan University of Science and Technology, Luoyang 471023, China

² Department of Automatic Control, Robotics and Fluid Technique, Faculty of Mechanical and Civil Engineering, University of Kragujevac, 36000 Kraljevo, Serbia

switching mechanism is proposed in [20] to make up for the shortcomings of DT and ADT switching mechanisms. More specifically, for the PDT switching mechanism (PDTSM), there exist infinite disjoint intervals (called τ -Portion) in which only one switching occurs, whose length is not less than the dwell time τ_p , and the portion between two consecutive τ -Portion is called T -Portion whose length is no greater than the persistence period T_p , where the subsystems can arbitrarily switch [21, 22]. Nevertheless, one point to be noted from the references [21, 22] on the PDTSM is that the results are feasible only under switched ordinary differential equation (ODE) systems. It is well-known that since switched RDSs can be applied to describe many complex systems that cannot be captured by switched ODE systems, such as the temperature control systems of semiconductor power chips [12]. Therefore, it is meaningful to extend PDTSM to switched RDSs.

With the remarkable advances in networked control systems [23–31], the control implementation of RDSs has been rapidly networked in control areas such as intelligent robot control [32] and chemical catalytic control [1]. On this trend, the design of networked control for RDSs has yielded a wealth of research results. To mention a few, a class of stochastic sampled-data control was studied in [33]; Selivanov and Fridman in [34], and Song et al. in [1] investigated novel design methods for point measurement and pointwise control, respectively, which have outstanding advantages in terms of reliability, low measurement costs, and ease transmission. However, it should be pointed out that the effect of bandwidth limitations is ignored in the above results [1, 33, 34]. Given the data to be transmitted, a fairly novel hysteresis quantizer with the advantages of avoiding controller chattering and improving bandwidth utilization was developed in [35, 36]. Still, despite the advantages of hysteresis quantization, it is an objective fact that quantization has a negative impact on system's performance [37]. Therefore, it makes sense to make a trade-off between the quantitative effect and the performance of the system. To the best of our knowledge, research results on the quantified control for switched RDSs with PDTSM, especially integrating the above trade-off, are not currently available, which stimulates the research interest of this work.

On the other hand, the existing work on stability analysis of switched systems mainly focused on two traditional ones: asymptotic stability [38] and exponential stability [39]. Unfortunately, these traditional stabilities have more rigorous restrictions and may be not always applicable in various dynamical systems, such as stochastic systems [40] and switched systems [41], where the systems' states remaining bounded within a certain rate of convergence [called exponential input-to-state stability (ISS)] is sufficient but do not necessarily converge to the equilibrium point. Nonetheless, up to now, despite the results have been achieved in the field of

switched ODE systems [41, 42], the problem of exponential ISS of switched RDSs remains a huge room for improvement due to the complexity and uniqueness of switched RDSs, which encourages us to make new attempts in the field.

Inspired by the above discussion, in terms of hysteresis quantization, this paper proposes a pointwise control method for the switched RDSs with PDTSM. The specific contributions of this article are emphasized as follows.

- Unlike previous studies biased toward the modeling approach of ODE systems [43, 44], RDSs [1, 8], and switched ODE systems [45–48], this article proposes a more extensive model of switched RDSs that can characterize more complex dynamical systems. Furthermore, this work makes the first step to extend the PDTSM to represent the switching rules possessed by subsystems, which enhances the proposed method's applicability compared to the DT and ADT switching mechanisms.

- This paper proposes a unified framework for switched RDS's signal measurement, transmission, and control. Specifically, different from [23, 25, 26], this work develops a combined point measurement and pointwise control approach, which effectively minimizes the quantities of sensors and actuators. Furthermore, in contrast to [35, 36], we propose the hysteresis quantization with a small parameter to balance the quantitative effect and system's performance while avoiding the controller's chattering and improving the bandwidth utilization.

- In practice, different from the asymptotic stability [38] and exponential stability [39], since the states of numerous systems are not strictly required to converge to the equilibrium point, this work attempts to formulate a relatively novel exponential ISS criteria for the switched RDSs with PDTSM, in which the systems' states only need to remain bounded with certain convergence rate.

Notations: $\text{int}[\aleph]$ denotes the maximal integer less than \aleph . Moreover, for the convenience of expression, define $\phi_t(x, t) = \frac{\partial \phi(x, t)}{\partial t}$, $\phi_x(x, t) = \frac{\partial \phi(x, t)}{\partial x}$, $\phi_{xt}(x, t) = \frac{\partial^2 \phi(x, t)}{\partial x \partial t}$, and $\phi_{xx}(x, t) = \frac{\partial^2 \phi(x, t)}{\partial x^2}$. The other notations are similar to [1] and are not repeated here.

Preliminaries and problem statements

System formulation

Consider the switched RDSs with PDTSM as follows:

$$\phi_t(x, t) = \Upsilon_{\theta(t)} \phi_{xx}(x, t) + \Lambda_{\theta(t)}(x) \phi(x, t) + g(x) u_{\theta(t)}, \quad (1)$$

subject to the initial condition

$$\phi(x, 0) = \phi_0(x), \quad (2)$$

and boundary conditions

$$\phi_x(l_1, t) = 0, \phi_x(l_2, t) = 0, \tag{3}$$

where $\phi(x, t) \in \mathcal{H}^n$ denotes the systems' state at the position $x \in [l_1, l_2]$ and time $t \in [0, \infty)$. $\theta(t) : [0, \infty) \rightarrow \mathbb{J} \triangleq \{1, 2, 3, \dots, M\}$ is the PDT switching signal, which is assumed to be a piecewise constant function and right-continuous, and M is the amount of subsystems. For convenience, let $\theta(t) = j$. Therefore, systems (1) is rewritten as

$$\phi_t(x, t) = \Upsilon_j \phi_{xx}(x, t) + \Lambda_j(x) \phi(x, t) + g(x) u_j, \tag{4}$$

where for any $j \in \mathbb{J}$, $\Upsilon_j \in \mathbb{R}^n$ is a known constant matrix, and $\Lambda_j(x)$ is a polynomial function with $\bar{\Lambda}_j \triangleq \max_{x \in [l_1, l_2]} \Lambda_j(x)$. The interval $[l_1, l_2]$ is divided into L subintervals. x_p and x_{p+1} represent the terminal points of the subinterval, $p \in \mathbb{P} \triangleq \{0, 1, \dots, L-1\}$. $\Delta_p \triangleq x_{p+1} - x_p$ represents the length between the two terminal points and $\bar{x}_p = \frac{x_p + x_{p+1}}{2}$ denotes the midpoint of the subinterval. The control input u_j is defined as $u_j \triangleq \text{col}[u_{j0} \ u_{j1} \ \dots \ u_{j(L-1)}]$, where $u_{jp} = \text{col}[u_{jp1} \ u_{jp2} \ \dots \ u_{jpn}]$. $g(x) \triangleq [g_0(x) \ g_1(x) \ \dots \ g_{L-1}(x)]$ with $g_p(x) \triangleq \delta(x - \bar{x}_p) g_p$ and g_p is a known scalar. Dirac delta function $\delta(x - \bar{x}_p)$ satisfies

$$\delta(x - \bar{x}_p) = \begin{cases} 0, & x \neq \bar{x}_p, \\ \infty, & x = \bar{x}_p. \end{cases}$$

With the above analysis, it is obtained that the space x is divided into L subintervals. The measurement of state information and the implementation of control signals are performed only at the midpoint \bar{x}_p , $p \in \mathbb{P}$ of each subinterval, which can largely reduce the number of sensors and actuators compared to the full domain control. Next, the pointwise controller is provided as follows:

$$u_{jp}(\bar{x}_p, t) = -K_{jp} \phi(\bar{x}_p, t), \tag{5}$$

where $K_{jp} > 0 \in \mathbb{R}^n$ ($j \in \mathbb{J}$, $p \in \mathbb{P}$) is the controller gain matrix that needs to be determined.

With the above point measurement and pointwise control, we obtain a control signal in the form of (5). However, during the long-distance transmission of the control signal to the actuators, the bandwidth limitation is a non-negligible problem. Therefore, we dedicate ourselves on improving the utilization of network bandwidth in the following.

Hysteresis quantizer

Indeed, the process of signal transmission over long distances is inevitably restricted by the fact that the bandwidth of the

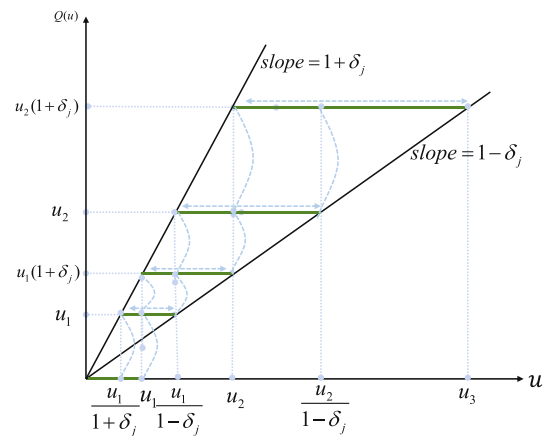


Fig. 1 Map of $Q(u)$ for $u > 0$

transmission channel has a limited capacity. Therefore, the following hysteresis quantizer is utilized [49]:

$$Q(u) = \begin{cases} u^\sigma \operatorname{sgn}(u), & \frac{u^\sigma}{1+\delta_j} < |u| \leq u^\sigma, \dot{u} < 0, \text{ or} \\ & u^\sigma < |u| \leq \frac{u^\sigma}{1-\delta_j}, \dot{u} > 0 \\ u^\sigma (1 + \delta_j) \operatorname{sgn}(u), & u^\sigma < |u| \leq \frac{u^\sigma}{1-\delta_j}, \dot{u} < 0, \text{ or} \\ & \frac{u^\sigma}{1-\delta_j} < |u| \leq \frac{u^\sigma (1+\delta_j)}{(1-\delta_j)}, \dot{u} > 0 \\ 0, & 0 \leq |u| < \frac{\zeta_j}{1+\delta_j}, \dot{u} < 0 \text{ or} \\ & \frac{\zeta_j}{1+\delta_j} \leq u \leq \zeta_j, \dot{u} > 0, \\ Q(u(t^-)), & \dot{u} = 0, \end{cases} \tag{6}$$

where $u^\sigma = v_j^{(1-\sigma)} \zeta_j$ with $\sigma \in \mathbb{N}^+$. The constants $v_j \in (0, 1)$ and ζ_j denote the quantizer density and the range of quantizer's dead-zone, respectively. The mode-dependent parameter δ_j satisfies $\delta_j = \frac{1-v_j}{1+v_j} \in (0, 1)$. The value of quantizer $Q(u)$ is in the set $\mathbb{Q} = \{0, \pm u^\sigma, \pm u^\sigma (1 + \delta_j)\}$.

Remark 1 The hysteresis quantizer not only outperforms the logarithmic quantizer in the number of additional levels of quantization, but also effectively avoids the phenomenon of controller chattering caused by the logarithmic quantizer [35]. As shown in Fig. 1, when the value $Q(u)$ of the hysteresis quantizer transitions from one level to another, there exists some dwell time before the new transition level appears, which avoids the controller's chattering.

To analyze the hysteresis quantizer's effect more intuitively, the hysteresis quantizer $Q(u)$ is reformulated as follows:

$$Q(\phi(\bar{x}_p, t)) = (1 - \varrho) \phi(\bar{x}_p, t) + \varrho e(\bar{x}_p, t), \tag{7}$$

where $0 < \varrho < 1$ is a given scalar, $e(\bar{x}_p, t)$ is a newly defined error variable.

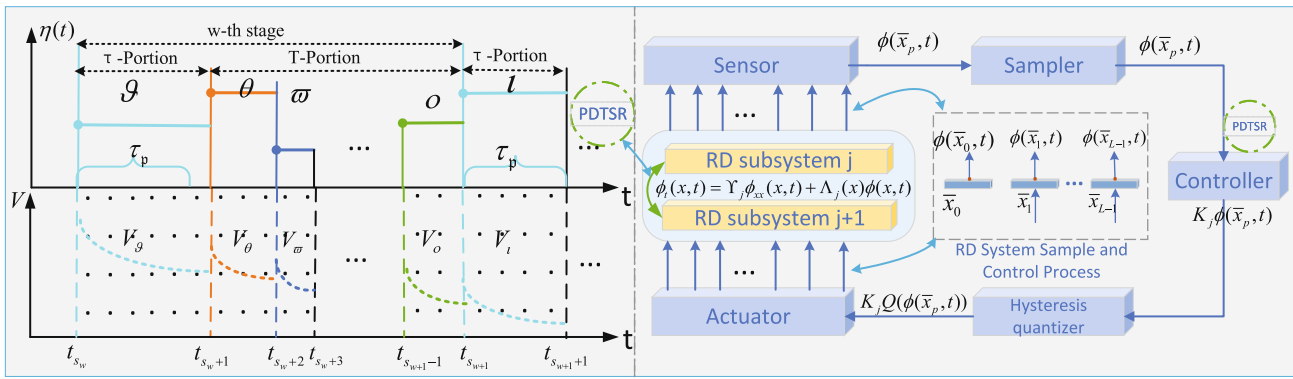


Fig. 2 Structural diagram of the proposed control scheme

Remark 2 In [35, 36], the hysteresis quantizer needs to satisfy $Q(\phi(\bar{x}_p, t)) = \phi(\bar{x}_p, t) - e(\phi(\bar{x}_p, t))$. In contrast, the hysteresis quantizer in this paper is improved to a linear combination of $\phi(\bar{x}_p, t)$ and $e(\phi(\bar{x}_p, t))$ depending the parameter ϱ , and by adjusting which can make a balance between the quantitative effect and the system’s performance.

Then, based on [49], the hysteresis quantizer is set as

$$|Q(\phi(\bar{x}_p, t)) - \phi(\bar{x}_p, t)| \leq \delta_j |\phi(\bar{x}_p, t)| + \zeta_j, \tag{8}$$

based on which, the control signal (5) is reformulated as

$$u_{jp}(\bar{x}_p, t) = -K_{jp}Q(\phi(\bar{x}_p, t)). \tag{9}$$

Combining (4), (7) and (9), the closed-loop switched RDSs has the following form:

$$\begin{aligned} \dot{\phi}_i(x, t) = & \Upsilon_j \phi_{xx}(x, t) + \Lambda_j(x)\phi(x, t) \\ & - g_p(x)K_{jp} \{ (1 - \varrho)\phi(\bar{x}_p, t) + \varrho e(\bar{x}_p, t) \}. \end{aligned} \tag{10}$$

To facilitate the subsequent analysis, the PDTSM should be described in detail.

PDTSM

Definition 1 (see [21]) The switching signal $\theta(t)$ obeys the PDTSM if there exist two positive numbers τ_p and T_p such that the following three conditions hold simultaneously:

- There are infinite and disjoint alternating intervals, i.e., the τ -Portion and the T -Portion.
- Each disjoint τ -Portion is not less than τ_p in length with the switching signal $\theta(t)$ being a constant value in these intervals.
- The length of each disjoint T -Portion is no longer than T_p . In the T -Portion, the switching signal $\theta(t)$ can switch arbitrarily, but the dwell time cannot exceed τ_p .

Figure 2 displays the PDT switching process and the variation of the energy function, where $t_{s_w}, t_{s_w+1}, t_{s_w+2}, \dots, t_{s_w+1+1}$ are the switching moments. Additionally, the energy function of the system in different subsystems ϑ and θ is represented by V_ϑ and V_θ at moments t_{s_w} and t_{s_w+1} , respectively. The whole stage w consists of τ -Portion and T -Portion. it is evident from Fig. 2 that the PDT switching signal is composed of numerous stages, and each stage comprises two portions: τ -Portion and T -Portion. In the τ -Portion, only one subsystem with a running time no less than dwell time τ_p is activated. In the T -Portion, these switchings can be arbitrary. Furthermore, for $w \in \mathbb{Z}^+$ and $n \in \mathbb{Z}^+$, the total running time \mathcal{T}_{RT-w} in a T -Portion of the w -th stage satisfies:

$$\mathcal{T}_{RT-w} = \sum_{n=1}^{\Upsilon(t_{s_w+1}, t_{s_w+1})} T(t_{s_w+n}, t_{s_w+n+1}) \leq T_p,$$

which means that the running time of the $T - Portion$ in stage w does not exceed T_p .

Remark 3 The superiority of the PDTSM: DT switching signal demands that the subsystem’s running time is not less than a fixed time constant τ_{DT} ; the switching times of ADT switching signal should satisfy $N(t, l) \leq \frac{l-t}{\tau_{ADT}} + N_0$, where l, τ_{ADT} and N_0 are positive numbers, which leads to the switching frequency of ADT switching mechanism is limited. Furthermore, if the T -Portion of the PDTSM is reduced to zero, the PDT signal can be simplified to a DT signal; if the persistence period of the T -Portion and the switching frequency of the PDT signal are reasonably limited, the PDT signal can be decreased to an ADT signal. Therefore, compared with the DT and ADT switching signals, PDTSM might have stronger applicabilities, which are demonstrated by the fact that it not only can describe the switching process that can be depicted by the DT and ADT switching mechanisms, but also can characterize the fast-switching phenomenon that the DT and ADT switching mechanisms can not.

Control objectives: For the investigated closed-loop switch-ed RDSs (10) with PDTSM, the focus of this work is primarily on the design of a hysteresis quantized point-wise controller to enable the closed-loop system to achieve exponential ISS. To further elaborate the proposed control strategy, the system diagram is shown in Fig. 2.

Before deriving the main results, some useful lemmas are provided in the following.

Lemma 1 (see [22]) *In the PDTSM, the times of switching in the $T -$ Portion are limited and do not produce Zeno behavior. Specifically, the switching times $C(v, t)$ in $[v, t)$ with $v > 0$ satisfy the following expression:*

$$0 \leq C(v, t) \leq \left(\left\lceil \frac{t - v}{T_p + \tau_p} \right\rceil + 1 \right) (\text{int}[T_p \cdot f] + 1).$$

Lemma 2 (see [50]) *The average switching frequency f_w of the PDTSM has the following form:*

$$f_w = \frac{C(t_{s_w+1}, t_{s_w+1})}{T_w}, r \in \mathbb{Z}^+,$$

where $1/f_w, T_w$ denote the each switching’s average length, the running time of the subsystem in the w -th stage, respectively. $C(t_{s_w+1}, t_{s_w+1})$ represents the switching times in the T -Portion. $f \triangleq \max\{f_w\}, 1/f \triangleq \min\{1/f_w\} \leq \max\{1/f_w\} < \tau_p$.

Main results

In this section, we first perform stability analysis for the target systems (10). Then, the control objectives are completed based on the obtained results.

Stability analysis

Theorem 3 *Preset positive scalars $\alpha, \Delta_p, g_p, \lambda_j, \delta_j, T_p, f, \tau_p$, and $\gamma > 1, 0 < \varrho < 1$, and provided that there exist positive matrices $K_{jp}, P_j, j, i \in \mathbb{J}(j \neq i)$ and $p \in \mathbb{P}$ such that*

$$\Xi_j = \begin{bmatrix} \Psi_{1j} & \Psi_{2j} & \Psi_{4j} \\ * & \Psi_{3j} & \varrho^2 \lambda_j \\ * & * & -\varrho^2 \lambda_j I \end{bmatrix} < 0,$$

where

$$\Psi_{1j} = 2P_j \bar{\Lambda}_j + \alpha P_j - \frac{1}{\Delta_p} 2(1 - \varrho) P_j g_p K_{jp} + 2\lambda_j \delta_j^2 - \varrho^2 \lambda_j,$$

$$\Psi_{2j} = -\frac{1}{\Delta_p} P_j g_p K_{jp} + 2\lambda_j \delta_j^2 - \varrho^2 \lambda_j,$$

$$\Psi_{3j} = -2 \frac{\pi^2}{\Delta_p^2} P_j \Upsilon_j + 2\lambda_j \delta_j^2 - \varrho^2 \lambda_j,$$

$$\Psi_{4j} = -\varrho \frac{1}{\Delta_p} P_j g_p K_{jp} + \varrho^2 \lambda_j,$$

$$P_j \leq \gamma P_i,$$

then the closed-loop switched RDSs (10) can achieve exponential ISS for the PDTSM satisfying

$$\beta = (T_p f + 1) \ln \gamma - \alpha \left(\frac{1}{f} + \tau_p \right) < 0.$$

Proof Step 1. Constructing the following Lyapunov function for stability analysis:

$$V_j(t) = \int_{l_1}^{l_2} \phi^T(x, t) P_j \phi(x, t) dx. \tag{11}$$

Differentiating $V_j(t)$ in (11) with respect to time t and combining (10), the following expression is obtained

$$\begin{aligned} \dot{V}_j(t) = & 2 \int_{l_1}^{l_2} \phi^T(x, t) P_j \{ \Upsilon_j \phi_{xx}(x, t) + \Lambda_j(x) \phi(x, t) \\ & - g_p(x) K_{jp} \{ (1 - \varrho) \phi(\bar{x}_p, t) + \varrho e(\bar{x}_p, t) \} \} dx. \end{aligned} \tag{12}$$

According to the boundary conditions (3) and the integration by parts, we get

$$\begin{aligned} & 2 \int_{l_1}^{l_2} \phi^T(x, t) P_j \Upsilon_j \phi_{xx}(x, t) dx \\ & = -2 \int_{l_1}^{l_2} \phi_x^T(x, t) P_j \Upsilon_j \phi_x(x, t) dx. \end{aligned} \tag{13}$$

By defining $m(x, t) = \phi(\bar{x}_p, t) - \phi(x, t)$ and based on Wirtinger’s inequalities, it follows that

$$\begin{aligned} & -2 \int_{l_1}^{l_2} \phi_x^T(x, t) P_j \Upsilon_j \phi_x(x, t) dx \\ & \leq -2 \sum_{p=0}^{L-1} \frac{\pi^2}{\Delta_p^2} \int_{x_p}^{x_{p+1}} m^T(x, t) P_j \Upsilon_j m(x, t) dx. \end{aligned} \tag{14}$$

Similar to (14), the following expression is generated

$$\begin{aligned} & -2 \sum_{p=0}^{L-1} \frac{1}{\Delta_p} \int_{x_p}^{x_{p+1}} \phi^T(x, t) P_j g_p K_{jp} \\ & \quad \times \{ (1 - \varrho) \phi(\bar{x}_p, t) + \varrho e(\bar{x}_p, t) \} dx \\ & = -2 \sum_{p=0}^{L-1} \frac{1}{\Delta_p} \int_{x_p}^{x_{p+1}} \phi^T(x, t) P_j g_p K_{jp} \{ (1 - \varrho) m(x, t) \} \end{aligned}$$

$$+(1 - \varrho)\phi(x, t) + \varrho e(\bar{x}_p, t)\} dx. \tag{15}$$

Then, along with (7) and integrating (11)–(15), one can derive

$$\dot{V}_j(t) + \alpha V_j(t) \leq \sum_{p=0}^{L-1} \int_{x_p}^{x_{p+1}} \varsigma^T \Xi_j \varsigma dx + 2\lambda_j \zeta_j^2, \tag{16}$$

where $\varsigma = \text{col}[\phi(x, t), m(x, t), e(\bar{x}_p, t)]$.

Step 2. Designing proper PDT switching signal.

Considering $\Xi_j < 0$, (16) ensures that

$$\dot{V}_j(t) + \alpha V_j(t) \leq 2\lambda_j \zeta_j^2. \tag{17}$$

Using Lemma 4 in [51] and making use of the fact that $P_j \leq \gamma P_i$ we can get

$$V_{\theta(t_{s_{w+1-1}})}(t) \leq \gamma e^{-\alpha(t-t_{s_{w+1-1}})} V_{\theta(t_{s_{w+1-2}})}(t_{s_{w+1-1}}) + \int_{t_{s_{w+1-1}}}^t e^{-\alpha(t-v)} 2\lambda_j \zeta_j^2 dv. \tag{18}$$

Analogous to (18), the following expression is produced

$$V_{\theta(t_{s_{w+1-2}})}(t_{s_{w+1-1}}) \leq e^{-\alpha(t_{s_{w+1-1}}-t_{s_{w+1-2}})} V_{\theta(t_{s_{w+1-2}})}(t_{s_{w+1-2}}) + \int_{t_{s_{w+1-2}}}^{t_{s_{w+1-1}}} e^{-\alpha(t-v)} 2\lambda_j \zeta_j^2 dv. \tag{19}$$

Substituting (19) into (18), we derive that

$$V_{\theta(t_{s_{w+1-1}})}(t) \leq \gamma e^{-\alpha(t-t_{s_{w+1-2}})} V_{\theta(t_{s_{w+1-2}})}(t_{s_{w+1-2}}) + \gamma \int_{t_{s_{w+1-2}}}^{t_{s_{w+1-1}}} e^{-\alpha(t-v)} 2\lambda_j \zeta_j^2 dv + \int_{t_{s_{w+1-1}}}^t e^{-\alpha(t-v)} 2\lambda_j \zeta_j^2 dv. \tag{20}$$

Then, iterating (20) from t to t_{s_w} , we can get

$$V_{\theta(t_{s_{w+1-1}})}(t) \leq \gamma^C(t_{s_w}, t) e^{-\alpha(t-t_w)} V_{\theta(t_{s_w})}(t_{s_w}) + \gamma^C(t_{s_w}, t) \int_{t_{s_w}}^t e^{-\alpha(t-v)} 2\lambda_j \zeta_j^2 dv \leq \gamma^C(t_{s_w}, t) e^{-\alpha(t-t_{s_w})} V_{\theta(t_{s_w})}(t_{s_w}) + 2\gamma^C(t_{s_w}, t) \alpha^{-1} \lambda_j \zeta_j^2, \tag{21}$$

where $C(t_{s_w}, t)$ denotes the switching times in $[t_{s_w}, t)$.

Next, define the two variables T_w and τ^p in the w stage:

$$\begin{cases} T_w \triangleq t - t_{s_w+1}, \\ \tau^p \triangleq t_{s_w+1} - t_{s_w}. \end{cases} \tag{22}$$

Combining Lemmas 1–2 and (22), the following inequality is given by

$$V_{\theta(t_{s_{w+1-1}})}(t) \leq \gamma^{T_p f+1} e^{-\alpha(\frac{1}{f}+\tau_p)} V_{\theta(t_{s_w})}(t_{s_w}) + 2\gamma^{T_p f+1} \alpha^{-1} \lambda_j \zeta_j^2. \tag{23}$$

To simplify the representation, the following definitions are provided

$$\gamma^{T_p f+1} e^{-\alpha(\frac{1}{f}+\tau_p)} \triangleq e^\beta < 1, \tag{24}$$

then, by a series of iterations and recursions, the following expressions hold

$$V_{\theta(t_{s_{w+1-1}})}(t) \leq \frac{1 - e^{(w+1)\beta}}{1 - e^\beta} \gamma^{T_p f+1} \alpha^{-1} 2\lambda_j \zeta_j^2 + e^{w\beta} V_{\theta(t_{s_1})}(t_{s_1}). \tag{25}$$

Define $\tilde{\lambda}(P_j) \triangleq \min_{j \in \mathbb{J}} \{\lambda_{\min}(P_j)\}$. According to (11), we can deduce that

$$V_j(t) \geq \tilde{\lambda}(P_j) \int_{t_1}^{t_2} \phi^T(x, t) \phi(x, t) dx = \tilde{\lambda}(P_j) \|\phi(x, t)\|^2, \forall j \in \mathbb{J},$$

Furthermore, due to $\theta(t_{s_{w+1-1}}) \in \mathbb{J}$, we can get

$$V_{\theta(t_{s_{w+1-1}})}(t) \geq \tilde{\lambda}(P_j) \|\phi(x, t)\|^2. \tag{26}$$

Now, combining (25) and (26), we obtain the state of the system satisfies

$$\|\phi(x, t)\|^2 \leq \tilde{\lambda}^{-1}(P_j) \left\{ (e^\beta)^w \tilde{\lambda}(P_j) \|\phi(x, 0)\|^2 + \frac{1 - (e^\beta)^{w+1}}{1 - e^{2\beta}} \gamma^{T_p f+1} \alpha^{-1} 2\lambda_j \zeta_j^2 \right\}. \tag{27}$$

Inspired by [51], it can be concluded that

$$\frac{t - t_{s_1}}{T_p + \tau_p} + 1 \leq w. \tag{28}$$

Therefore, substituting (28) into (27), we get

$$\|\phi(x, t)\|^2 \leq \tilde{\lambda}^{-1}(P_j) \left\{ e^{\beta(0.25T_p t + 0.5)} \tilde{\lambda}(P_j) \|v(x, 0)\|^2 + \frac{1}{1 - e^\beta} \gamma^{T_p f+1} \alpha^{-1} 2\lambda_j \zeta_j^2 \right\}. \tag{29}$$

Based on (11), the following equation can be generated

$$\tilde{\lambda}(P_j) \|\phi(x, t)\|^2 \leq V_j(t) \leq \bar{\lambda}(P_j) \|\phi(x, t)\|^2. \tag{30}$$

where $\bar{\lambda}(P_j) \triangleq \max_{j \in \mathbb{J}} \{\lambda_{\min}(P_j)\}$.

By defining $\hat{\lambda}(P_j) \triangleq \bar{\lambda}(P_j)\bar{\lambda}^{-1}(P_j)$ and combining (30)–(31), one obtains

$$V_j(t) \leq \hat{\lambda}(P_j) \left\{ e^{\beta(0.25T_p t + 0.5)} \hat{\lambda}(P_j) V_j(0) + \frac{1}{1 - e^\beta} \gamma^{T_p f + 1} \alpha^{-1} 2\lambda_j \zeta_j^2 \right\}. \tag{31}$$

Therefore, based on (31) and the definition of exponential ISS in [49], it is concluded that the closed-loop switched RDSs (10) with PDTSM are exponential ISS. The proof is completed. ■

Controller design

Notably, Theorem 3 only offers sufficient conditions for the exponential ISS of the closed-loop switched RDSs (10). To derive the controller’s gain parameters, the following Theorem can be drawn by applying the decoupling technique.

To this end, by defining $\tilde{K}_{jp} = P_j K_{jp}$, we can get the controller’s gain parameter satisfies

$$K_{jp} = \tilde{K}_{jp} P_j^{-1}, j \in \mathbb{J}, p \in \mathbb{P}.$$

Employing (35), the controller gains can be yielded through solving the inequalities in Theorem 4.

Theorem 4 *Given positive constants $\alpha, f, \Delta_p, g_p, \lambda_j, \delta_j, T_p, \tau_p$, and $\gamma > 1, 0 < \varrho < 1$, the system (10) is exponential ISS, if there exist matrices $\tilde{K}_{jp} > 0, P_j > 0, j, i \in \mathbb{J}(j \neq i)$ and $p \in \mathbb{P}$, the following inequalities hold:*

$$\tilde{\Xi}_j = \begin{bmatrix} \tilde{\Psi}_{1j} & \tilde{\Psi}_{2j} & \tilde{\Psi}_{4j} \\ * & \Psi_{3j} & \varrho^2 \lambda_j \\ * & * & -\varrho^2 \lambda_j I \end{bmatrix} < 0,$$

$$\beta = (T_p f + 1) \ln \gamma - \alpha \left(\frac{1}{f} + \tau_p \right) < 0,$$

with

$$\begin{aligned} \tilde{\Psi}_{1j} &= 2P_j \bar{\Lambda}_j + \alpha P_j - \frac{1}{\Delta_p} 2(1 - \varrho) g_p \tilde{K}_{jp} \\ &\quad + 2\lambda_j \delta_j^2 - \varrho^2 \lambda_j, \\ \tilde{\Psi}_{2j} &= -\frac{1}{\Delta_p} g_p \tilde{K}_{jp} + 2\lambda_j \delta_j^2 - \varrho^2 \lambda_j, \\ \tilde{\Psi}_{4j} &= -\frac{1}{\Delta_p} g_p \tilde{K}_{jp} + \varrho^2 \lambda_j, \\ P_j &\leq \gamma P_i, \end{aligned}$$

where Ψ_{3j} is given in Theorem 3 and the controller’s gain matrix satisfies $K_{jp} = \tilde{K}_{jp} P_j^{-1}$.

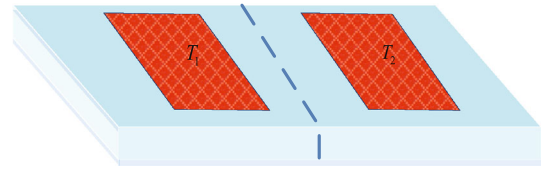


Fig. 3 Structure diagram of chips

Table 1 Model parameters

Notation	Meaning	Unit
ϖ	Heat conductivity	W/(m · K)
ρ	Material density	Kg/m ³
c_s	Specific heat	J/(kg · K)
\mathfrak{T}	Chip thickness	μm
$a(x)$	Surface area of the chip	(μm) ²

Chip temperature control

To validate the effectiveness of the proposed control method, an application example i.e., temperature control of power semiconductor chips is given in this section.

The considered power semiconductor chip consists of two DMOS-arrays as shown in Fig. 3. Generally, the internal structure of these two DMOS-arrays can be disregarded for simplicity [12]. The epitaxial layer is assumed to be the only heating layer within the DMOS-array. The heat generated from the chips regions T_1 and T_2 propagates downward in its solid-state material. Thus, the temperature system of the power semiconductor chip can be described with the following RDS model:

$$\mathfrak{R}_t(x, t) = \Upsilon \mathfrak{R}_{x,x}(x, t) + \Lambda(x) \mathfrak{R}(x, t) + g(x)u, \tag{32}$$

subject to the initial condition

$$\mathfrak{R}(x, 0) = \mathfrak{R}_0(x), \tag{33}$$

and boundary conditions

$$\mathfrak{R}_x(l_1, t) = 0, \mathfrak{R}_x(l_2, t) = 0, \tag{34}$$

where state $\mathfrak{R}(x, t)$ of the system represents the temperature of the semiconductor power chip. Υ and $\Lambda(x)$ denote the diffusion coefficient and thermal resistance of the chip with $\Upsilon = \varpi / (\rho \cdot c_s)$ and $\Lambda(x) = \mathfrak{T} / (\varpi \cdot a(x))$, respectively and their parameters are detailed in Table 1. Further, according to the thermal resistance formula, we can discover that the thermal resistance value is inversely proportional to the chip’s area.

Next, we consider that T_1 or T_2 generates heat. Since the heat conductivity ϖ is related to the physical structure of T_1

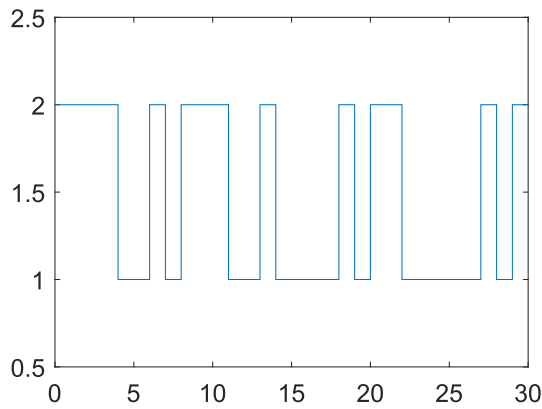


Fig. 4 Diagram of modal change of PDTSM

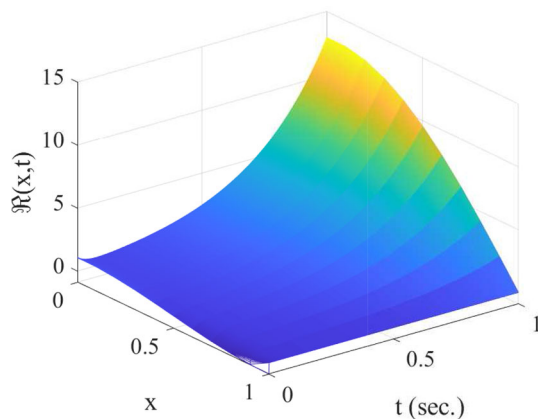


Fig. 5 Evolution trajectory of open-loop state

and T_2 , the changes of T_1 and T_2 result in the changes of ϖ . Furthermore, since the material and shape of the chip are fixed, the variations of ρ , c_s , \mathfrak{T} and $a(x)$, which are related to the material or shape of the chip, can be ignored. Therefore, Υ and $\Lambda(x)$ with the switching characteristics are rewritten as $\Upsilon_{\theta(t)} = \varpi_{\theta(t)}/(\rho \cdot c_s)$ and $\Lambda_{\theta(t)}(x) = \mathfrak{T}/(\varpi_{\theta(t)} \cdot a(x))$, respectively. Therefore, system (32) can be re-modeled to the switched RDS as follows

$$\mathfrak{R}_t(x, t) = \Upsilon_{\theta(t)}\mathfrak{R}_{xx}(x, t) + \Lambda_{\theta(t)}(x)\mathfrak{R}(x, t) + g(x)u_{\theta(t)}, \tag{35}$$

Inspired by [12], the parameters of the system (35) are chosen as follows: The number of system’s modes is chosen as 2, where the change of the modes is shown in Fig. 4. Next, the coefficients of the system corresponding to each mode are configured. When the mode is 1, $\Upsilon_1 = 1$, $\Lambda_1(x) = 5\exp(-0.1x^2) + 0.2$; when the mode is 2, $\Upsilon_2 = 2$, $\Lambda_2(x) = 2\exp(-x^2) + 1$. Select the initial condition of the system (35) satisfying $\mathfrak{R}_0(x) = 0.1 + \cos(\pi x)$. The corresponding open-loop system’s state evolution trajectory is shown in Figure. 5, where the state of the system is remarkably divergent.

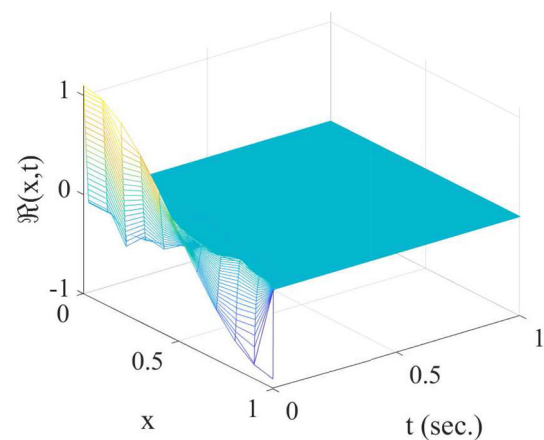


Fig. 6 Evolution trajectory of close-loop state

Therefore, based on the above analysis, it is necessary and meaningful to impose control on the investigated switched RDS (35). Initially, the space length $l_2 - l_1 = 1$ is divided into five intervals spaced by 0.2, then the midpoint of each interval are $\bar{x}_1 = 0.1$, $\bar{x}_2 = 0.3$, $\bar{x}_3 = 0.5$, $\bar{x}_4 = 0.7$, $\bar{x}_5 = 0.9$. Subsequently, by selecting parameters $j = 2$, $p = 5$, $\alpha = 0.6$, $f = 5$, $\gamma = 1.01$, $\Delta_p = 0.2$, $g_p = 63.5$, $\lambda_1 = 0.03$, $\lambda_2 = 0.035$, $T_p = 4$, $\tau_p = 3$, $v_1 = 0.002$, $v_2 = 0.0025$, $\zeta_1 = 0.002$, $\zeta_2 = 0.0025$, $\varrho = 0.15$, we obtain the controller gains as shown in (36) by solving the linear matrix inequalities in Theorem 4.

Then, the hysteresis quantified controller (9) is applied to the system (35). The evolution trajectories of the system’s state $\mathfrak{R}(x, t)$ and quantified control input (9) are shown in Figs. 6 and 7, respectively. According to Figs. 6 and 7, it can be concluded that the system (35) is rapidly stabilized.

$$K_{jp} = \begin{cases} 0.1523, & x = 0.1, p = 1, j = 1, \\ 0.1483, & x = 0.3, p = 2, j = 1, \\ 0.1270, & x = 0.5, p = 3, j = 1, \\ 0.1129, & x = 0.7, p = 4, j = 1, \\ 0.0655, & x = 0.9, p = 5, j = 1. \end{cases} \tag{36}$$

$$K_{jp} = \begin{cases} 0.2162, & x = 0.1, p = 1, j = 2, \\ 0.1734, & x = 0.3, p = 2, j = 2, \\ 0.1526, & x = 0.5, p = 3, j = 2, \\ 0.1268, & x = 0.7, p = 4, j = 2, \\ 0.0611, & x = 0.9, p = 5, j = 2. \end{cases}$$

Next, a logarithmic quantizer is utilized to highlight the advantages of the hysteresis quantizer employed in this paper. Specifically, Fig. 8 shows the trajectory of logarithmic quantified control input. It can be observed from Fig. 8 that the logarithmic quantizer causes controller chattering, which results in a longer time to achieve system’s stability.

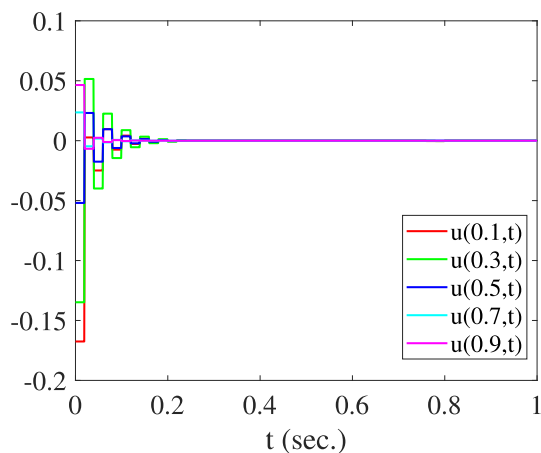


Fig. 7 Evolution curve of control input

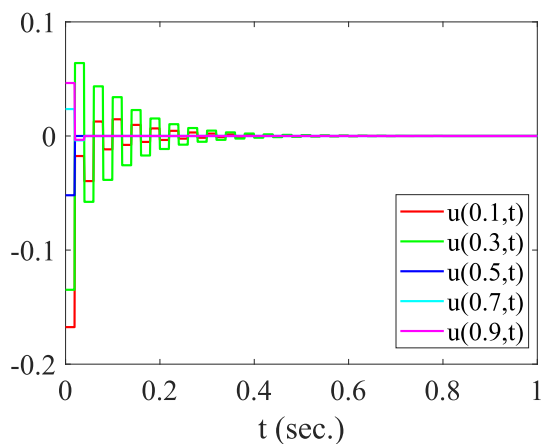


Fig. 8 Evolution curve of control input

Conclusions

This work has addressed the stabilization problem of switched RDSs. Specifically, the switchings between operating modes of the considered systems are consistent with the PDTSM, which is more general than the DT and ADT switching mechanisms. Further, by using the networked control framework of the point measurement, pointwise control and hysteresis quantizer with an adjustable parameter, the exponential ISS of the closed-loop switched RDSs is obtained. Finally, the applicability of the derived theoretical results is verified by the temperature control simulations of power semiconductor chips. The future work will expand the proposed methods to design the secure control strategy for the switched RDSs with network attacks. Meanwhile, to further improve the communication efficiency, we will extend the input quantization proposed in this paper to input–output quantization or input-state quantization.

Acknowledgements This work was supported in part by the National Natural Science Foundation of China under Grants 62203153 and

61976081, in part by the Natural Science Fund for Excellent Young Scholars of Henan Province under Grant 202300410127, in part by Key Scientific Research Projects of Higher Education Institutions in Henan Province under Grant 22A413001, in part by Top Young Talents in Central Plains under Grant Yuzutong (2021) 44, in part by Technology Innovative Teams in the University of Henan Province under Grant 23IRTSTHN012, in part by the Natural Science Fund for Young Scholars of Henan Province under Grant 222300420151, and in part by the Serbian Ministry of Education, Science and Technological Development (No. 451-03-47/2023-01/200108).

Open Access This article is licensed under a Creative Commons Attribution 4.0 International License, which permits use, sharing, adaptation, distribution and reproduction in any medium or format, as long as you give appropriate credit to the original author(s) and the source, provide a link to the Creative Commons licence, and indicate if changes were made. The images or other third party material in this article are included in the article's Creative Commons licence, unless indicated otherwise in a credit line to the material. If material is not included in the article's Creative Commons licence and your intended use is not permitted by statutory regulation or exceeds the permitted use, you will need to obtain permission directly from the copyright holder. To view a copy of this licence, visit <http://creativecommons.org/licenses/by/4.0/>.

References

1. Song X, Zhang Q, Zhang Y, Song S (2022) Fuzzy event-triggered control for PDE systems with pointwise measurements based on relaxed Lyapunov-Krasovskii functionals. *IEEE Trans Fuzzy Syst* 30(8):3074–3084
2. Wang J, Krstic M (2021) Adaptive event-triggered PDE control for load-moving cable systems. *Automatica* 129:109637
3. Katz R, Fridman E (2021) Sub-predictors and classical predictors for finite-dimensional observer-based control of parabolic PDEs. *IEEE Control Syst Letters* 6:626–631
4. Wang J (2019) Observer-based boundary control of semi-linear parabolic PDEs with non-collocated distributed event-triggered observation. *J Franklin Inst* 356(17):10405–10420
5. Zhang R, Zeng D, Park JH, Liu Y, Xie X (2020) Adaptive event-triggered synchronization of reaction-diffusion neural networks. *IEEE Trans Neural Netw Learn Syst* 32(8):3723–3735
6. Ren Y, Zhao Z, Ahn CK, Li H (2022) Adaptive fuzzy control for an uncertain axially moving slung-load cable system of a hovering helicopter with actuator fault. *IEEE Trans Fuzzy Syst* 30(11):4915–4925
7. Song X, Zhang Q, Song S, Ahn CK (2022) Sampled-data-based event-triggered fuzzy control for PDE systems under cyberattacks. *IEEE Trans Fuzzy Syst* 30(7):2693–2705
8. Pitarch JL, Rakhshan M, Mardani MM, Shasadeghi M (2018) Distributed saturated control for a class of semilinear PDE systems: an SOS approach. *IEEE Trans Fuzzy Syst* 26(2):749–760
9. Wang P, Katz R, Fridman E (2023) Constructive finite-dimensional boundary control of stochastic 1D parabolic PDEs. *Automatica* 148:110793
10. Wang Z, Zhang X, Wu H, Huang T (2023) Fuzzy boundary control for nonlinear delayed dpss under boundary measurements. *IEEE Trans Cybern* 53(3):1547–1556
11. Ahmed-Ali T, Lamnabhi-Lagarrigue F, Khalil HK (2023) High-gain observer-based output feedback control with sensor dynamic governed by parabolic PDE. *Automatica* 147:110664
12. Guan Y, Yang H, Jiang B (2019) Fault-tolerant control for a class of switched parabolic systems. *Nonlinear Anal Hybrid Syst* 32:214–227

13. Wu W, Li Y, Tong S (2021) Fuzzy adaptive tracking control for state constraint switched stochastic nonlinear systems with unstable inverse dynamics. *IEEE Trans Syst Man Cybern Syst* 51(9):5522–5534
14. Qi W, Zong G, Su S (2022) Fault detection for semi-Markov switching systems in the presence of positivity constraints. *IEEE Trans Cybern* 52(12):13027–13037
15. Peitz S, Klus S (2019) Koopman operator-based model reduction for switched-system control of PDEs. *Automatica* 106:184–191
16. Morse AS (1996) Supervisory control of families of linear set-point controllers-Part 1. Exact matching. *IEEE Trans Autom Control* 41(10):1413–1431
17. Hespanha JP, Morse AS (1999) Stability of switched systems with average dwell-time, in: *Proceedings of the 38th IEEE Conference on decision and control*, Phoenix, AZ, USA
18. Wang Y, Hu X, Shi K, Song X, Shen H (2020) Network-based passive estimation for switched complex dynamical networks under persistent dwell-time with limited signals. *J Franklin Inst* 357(15):10921–10936
19. Zhang L, Zhuang S, Shi P (2015) Non-weighted quasi-time-dependent H_∞ filtering for switched linear systems with persistent dwell-time. *Automatica* 54:201–209
20. Hespanha JP (2004) Uniform stability of switched linear systems: extensions of LaSalle's invariance principle. *IEEE Trans Autom Control* 49(4):470–482
21. Zhang L, Xu K, Yang J, Han M, Yuan S (2022) Transition-dependent bumpless transfer control synthesis of switched linear systems. *IEEE Trans Autom Control*. <https://doi.org/10.1109/TAC.2022.3152721>
22. Du D, Xu S, Cocquempot V (2018) Fault detection for nonlinear discrete-time switched systems with persistent dwell time. *IEEE Trans Fuzzy Syst* 26(4):2466–2474
23. Koga S, Karafyllis I, Krstic M (2021) Towards implementation of PDE control for Stefan system: input-to-state stability and sampled-data design. *Automatica* 127:109538
24. Ma B, Li Y (2022) Compensator-critic structure-based event-triggered decentralized tracking control of modular robot manipulators: theory and experimental verification. *Complex Intell Syst* 8:1913–1927
25. Wang Z, Wu H, Wang X (2020) Sampled-data fuzzy control with space-varying gains for nonlinear time-delay parabolic PDE systems. *Fuzzy Sets Syst* 392:170–194
26. Yu X, Lin Y (2016) Adaptive backstepping quantized control for a class of nonlinear systems. *IEEE Trans Autom Control* 62(2):981–985
27. Cheng J, Wu Y, Wu Z, Yan H (2022) Nonstationary filtering for fuzzy Markov switching affine systems with quantization effects and deception attacks. *IEEE Trans Syst Man Cybern Syst* 52(10):6545–6554
28. Su X, Wang C, Chang H, Yang Y, Assawinchaichote W (2021) Event-triggered sliding mode control of networked control systems with Markovian jump parameters. *Automatica* 125:109405
29. Xia Y, Zhang J, Jiang T, Gong Z, Yao W, Feng L (2021) Hatchensemble: an efficient and practical uncertainty quantification method for deep neural networks. *Complex & Intelligent Systems* 7:2855–2869
30. Wuthishuwong C, Traectler A (2017) Consensus-based local information coordination for the networked control of the autonomous intersection management. *Complex Intell Syst* 3:17–32
31. Li Z, Chang X, Park JH (2021) Quantized static output feedback fuzzy tracking control for discrete-time nonlinear networked systems with asynchronous event-triggered constraints. *IEEE Trans Syst Man Cybern Syst* 51(6):3820–3831
32. He W, Kang F, Kong L, Feng Y, Cheng G, Sun C (2022) Vibration control of a constrained two-link flexible robotic manipulator with fixed-time convergence. *IEEE Trans Cybern* 52(7):5973–5983
33. Li Q, Wang Z, Huang T, Wu H, Li H, Qiao J (2023) Fault-tolerant stochastic sampled-data fuzzy control for nonlinear delayed parabolic PDE systems. *IEEE Trans Fuzzy Syst*. <https://doi.org/10.1109/TFUZZ.2023.3235400>
34. Selivanov A, Fridman E (2016) Distributed event-triggered control of diffusion semilinear PDEs. *Automatica* 68:344–351
35. Song S, Park JH, Zhang B, Song X (2022) Composite adaptive fuzzy finite-time quantized control for full state-constrained nonlinear systems and its application. *IEEE Trans Syst Man Cybern Syst* 52(4):2479–2490
36. Li Y, Yang G (2019) Observer-based adaptive fuzzy quantized control of uncertain nonlinear systems with unknown control directions. *Fuzzy Sets Syst* 371:61–77
37. Liu W, Lim C-C, Shi P, Xu S (2017) Backstepping fuzzy adaptive control for a class of quantized nonlinear systems. *IEEE Trans Fuzzy Syst* 25(5):1090–1101
38. Hante FM Stability and optimal control of switching PDE-dynamical systems, arXiv preprint [arXiv:1802.08143](https://arxiv.org/abs/1802.08143)
39. Amin S, Hante FM, Bayen AM (2011) Exponential stability of switched linear hyperbolic initial-boundary value problems. *IEEE Trans Autom Control* 57(2):291–301
40. Ren W, Xiong J (2017) Stability analysis of impulsive stochastic nonlinear systems. *IEEE Trans Autom Control* 62(9):4791–4797
41. Wu X, Tang Y, Cao J (2019) Input-to-state stability of time-varying switched systems with time delays. *IEEE Trans Autom Control* 64(6):2537–2544
42. Zhang M, Zhu Q (2019) Input-to-state stability for non-linear switched stochastic delayed systems with asynchronous switching. *IET Control Theory Appl* 13(3):351–359
43. Sui S, Chen CP, Tong S (2023) A novel full errors fixed-time control for constraint nonlinear systems. *IEEE Trans Autom Control* 68(4):2568–2575
44. Wu W, Tong S (2022) Observer-based fixed-time adaptive fuzzy consensus DSC for nonlinear multiagent systems. *IEEE Trans Cybern*. <https://doi.org/10.1109/TCYB.2022.3204806>
45. Sui S, Chen CP, Tong S (2021) Neural-network-based adaptive DSC design for switched fractional-order nonlinear systems. *IEEE Trans Neural Netw Learn Syst* 32(10):4703–4712
46. Shen H, Xing M, Wu Z, Xu S, Cao J (2020) Multiobjective fault-tolerant control for fuzzy switched systems with persistent dwell time and its application in electric circuits. *IEEE Trans Fuzzy Syst* 28(10):2335–2347
47. Shi S, Fei Z, Wang T, Xu Y (2019) Filtering for switched T-S fuzzy systems with persistent dwell time. *IEEE Trans Cybern* 49(5):1923–1931
48. Yang Y, Chen F, Lang J, Chen X, Wang J (2021) Sliding mode control of persistent dwell-time switched systems with random data dropouts. *Appl Math Comput* 400:126087
49. Kang W, Wang X, Guo B (2022) Observer-based fuzzy quantized control for a stochastic third-order parabolic PDE system. *IEEE Trans Syst Man Cybern Syst* 53(1):485–494
50. Nie L, Cai B, Lu S, Qin H, Zhang L (2021) Finite-time switched LPV control of quadrotors with guaranteed performance. *J Franklin Inst* 358(14):7032–7054
51. Shen H, Huang Z, Cao J, Park JH (2020) Exponential \mathcal{H}_∞ filtering for continuous-time switched neural networks under persistent dwell-time switching regularity. *IEEE Trans Cybern* 50(6):2440–2449